Journal of Vacuum Science & Technology A

Internal chemical potential in mixed covalent-ionic photosensitive systems

Running title: Internal potential in covalent-ionic systems

Running Authors: Kot et al.

Małgorzata Kot[a)], Karsten Henkel and Dieter Schmeißer

Institute of Physics, Brandenburg University of Technology Cottbus-Senftenberg, Konrad-Zuse-Straße 1, 03046 Cottbus, Germany

[a)] Electronic mail: sowinska@b-tu.de

The internal chemical potential Γ of mixed covalent-ionic systems represents the potential differences between the covalent and the ionic intrinsic defect states located within the ionic gap. It is the key parameter to control the carrier densities, the stability regimes, and the photosensitive properties of materials. In this work, we describe first the quantitative analysis of the carrier densities in dependence on the internal potential $N^{\pi}(\Gamma)$ based on the common features of the electronic structure of mixed covalent-ionic materials. Subsequently, this method is applied on two mixed covalent-ionic materials, i.e., formamidinium lead triiodide and gallium oxide, as representatives of the respective families of perovskites (halides) and transparent conducting oxide thin films. Based on this analysis, the carrier densities as well as the photosensitivity mechanisms and the related specific properties of these materials in dependence on their internal chemical potential are discussed.

I. INTRODUCTION

Photosensitive materials as well as associated devices, such as photoabsorbers and solar cells, are well established in the literature.[1-5] In our previous works we presented that formamidinium lead triiodide ($FAPbI_3$, shorty FAPI)[6] and gallium oxide (Ga_2O_3)[7,8] photoactive materials are mixed covalent-ionic systems and their fundamental physical mechanisms can be described by the internal chemical potential Γ. It represents the potential differences between the covalent and the ionic intrinsic defect states located within the ionic gap. It is the key parameter to control the carrier densities, the stability regimes, and the photosensitive properties of materials[6,8]. Our approach[8] to use the chemical potential Γ for a quantitative analysis of the carrier densities $N^{\pi}(\Gamma)$ is a novel description of photosensitive systems that presents an alternative physical explanations for the carriers, their densities, and their loss mechanisms.

In this work, we briefly introduce the basics of our approach and compare two systems, FAPI and Ga_2O_3, as representatives of the material families of perovskites and transparent conducting oxides (TCOs) thin films, respectively. We demonstrate that these systems can be described as mixed covalent-ionic systems although they represent quite different classes of materials. The similarities[6-8] between both materials are striking and are based on common features appearing in their electronic structures and on the nature of the multi-atomic carriers. The quantitative analysis of their density defines the stability regimes of their photosensitivity and related limitations. This successful comparative approach enables new aspects for the discussion of some of the open issues that are still debated in the literature,[1,9-12] such as the origin and limits of photosensitivity, the achieved light induced carrier densities, and the mechanisms for degradation and losses.

Moreover, we demonstrate deviations from ohmic behavior reflected by combined ohmic-exponential characteristics or asymmetric I-V curves as observed in photoabsorbers and rectifying devices. The chemical potential determines the dipole-controlled dissociation of $B^{2\pi}$ BiPs in covalent-ionic systems, their stability regime, the performance limits, and the loss processes. It describes the transport in photosensitive perovskite and TCO materials by pairing and dissociation of $P^{1\pi}$ and/or $P^{3\pi}$ LaPs to $B^{2\pi}$ and/or $B^{4\pi}$, $B^{6\pi}$ BiPs and vice versa, where their density $N^{\pi}(\Gamma)$ exhibits an exponential dependence on the internal potential Γ, which is modified by the applied bias voltage (V_{bias}) and depends further on the ionicity factor f_i. The internal chemical potential Γ reflects the size of the ionic gap, the applied V_{bias}, and sums all internal dipoles contributions.

II. EXPERIMENTAL

The samples preparation as well as detailed experimental procedures are described in our previous works in detail[6,8,9,17].

III. RESULTS AND DISCUSSION

The basis of our explanations and the common aspect in all covalent-ionic systems is that their fascinating properties are caused by covalent interactions of defects located within the ionic energy gap as intrinsic defect states (IDS)[7,13,14]. Such intrinsic covalently bound defect states overcome the strong ionic system although they have an ionic basis, they exist as large polarons (LaPs) built by multi-atomic wave functions and their charge is fully screened by their polarization cloud[8]. We distinguish localized,

weakly localized, and mobile (delocalized) defect states that fill the ionic gap in the exciton, charge transfer (CT-), and bipolaron (BiP-) bands, respectively (see Fig. 1). The density of the mobile LaPs – as the main carriers – depends on the ionicity value f_i[15,16] (with $f_i < 1$) and is controlled by the internal potential Γ. This approach works well for all mixed covalent-ionic systems. Based on changes in the internal potential Γ, the corresponding changes in the density of the LaPs are used to describe possible applications.

A. Similarities in the electronic structure

In Fig. 1 the electronic structure of methyl ammonium lead triiodide (MAPI) – as a representative of the family of photosensitive perovskites – is compiled. The chemical potential Γ is based on the electronic structure which is characteristic for all covalent-ionic systems. Only the size of the ionic band gap and the ionicity value differ. Our analysis is based on the features of the electronic structure, and in particular, on the size of the ionic energy gap defined by the ionization (V_L) and affinity (V_U) levels and on the appearance of covalent intrinsic defect states located within it.[8] The IDS form extended bands and are populated by LaPs as carriers with different spatial and energetic localization; the mobile fraction populates the BiPs-band, the weakly localized states are in the CT-band, and the more localized in the exciton-band. The blue bars represent the valence states below V_L and beyond V_U. The covalent intrinsic defect states (CT-band (red area), BiP-band (green), exciton band (light-yellow bar)) are located within the ionic gap (Fig. 1b) as derived from the photoemission (red) and X-ray absorption (black) data taken at the N1s edge (resPES) of MAPI[18] (Fig. 1a). The partial occupation of the CT-band is indicated by the dark red triangle. The diagram also reflects the optical properties by the yellow arrows indicating

the photoluminescence data (PL)[1] and the creation of the light dipole V^{light} (ħω). The latter is created by absorption of light with 1.6 eV between the occupied (dark red triangle) and the empty states within the CT-band beyond the exciton band; the dotted thin red line marks the crossover of the spectroscopic data. These details of the electronic structure are very similar for several covalent-ionic systems. This facts is established for a series of systems such as Ga_2O_3[7,8], TiO_2[14], MAPI[18], FAPI[6], triple cation perovskite (TC)[6], WO_3[19,20] and ZnO[13], to name a few. These systems differ just in their width of the ionic gap and the f_i value. For all of them, the chemical potential is well defined and is used to determine the carrier densities quantitatively. However, within the chemical potential, differences arise for the individual critical values of V^{pair}, V*, and Γ* and these variations lead also to different pairing and dissociation behavior (to be described below).

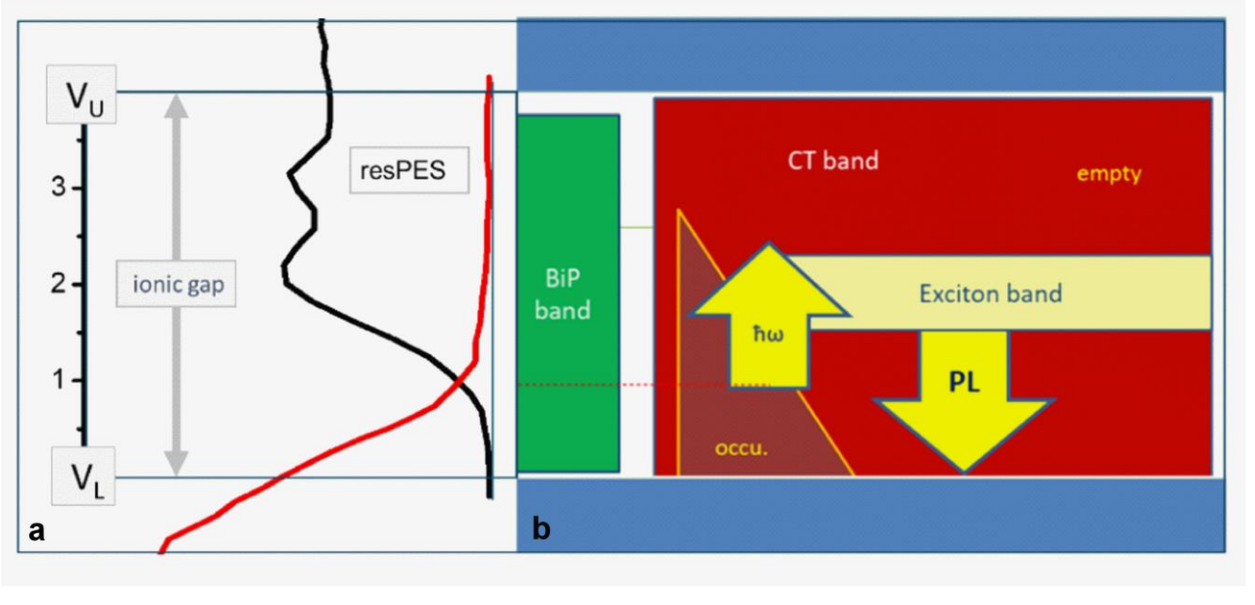

FIG. 1. The generalized band scheme of perovskite materials (b) with indicated bipolarons band (BiP band), charge transfer (CT) and exciton bands deduced from the resonant photoelectron spectroscopy data[18] of MAPI (a). This diagram illustrates the ionic gap

($E^{ionicgap}$ = 4.0eV) between the ionization potential (V_L) and the electron affinity level (V_U). All energy values (in eV) are referred to V_L=0 as indicated by the axis in Fig. 1a. The photoluminescence (PL)[1] and the light dipole V^{light} (ħω) are also illustrated in Fig. 1b.

B. Similarities in the carrier densities dependence on the chemical potential

The second striking similarity of hybrid perovskite and TCO materials is that the carrier density of the mobile charges can be derived quantitatively by the analysis of their I-V curves. It requires that the ionicity factor f_i of the analyzed material is smaller than 1. The f_i value can be experimentally assessed by e.g., spectroscopic features[13] such as core level shifts, width and relative intensities of defect bands (in Ga_2O_3 f_i = 0.9, in IGZO f_i = 0.7, in In_2O_3 f_i = 0.72, in SnO_2 f_i = 0.83, and in ZnO f_i = 0.81), and also by I-V curves in photosensitive perovskites[6] ($0.37 \leq f_i \leq 0.73$). Our quantitative analysis is based on the respective Γ value that describes the potential difference between covalent (BiP-band) and ionic charge reservoir (CT-band) subsystems, and includes the contribution of V_{bias} and all internal dipoles. We use the dimensionless and normalized internal potential Γ[8] as:

$$\Gamma = [(V_L - V^{\pi}) - V^0 + V_{bias}] / E_{ionicgap}. \quad (1)$$

In Eq. (1), the value of Γ reflects the position of the chemical potential within the ionic gap ($E_{ionicgap}$) refereed to V^0 (equilibrium) and Γ is maximal for $V_{bias} = V^0 + V_L$ and minimal for $V_{bias} = V^0 + V_U$. It varies with the applied bias potential V_{bias} and considers the sum of all internal dipoles V^{π} caused by vacancies (V^*), pairing equilibria (V^{pair}), or by light (V^{light}). The referred energy values of the ionization potential V_L, the electron

affinity level V_U, and the midgap position V^0 are all deduced from our earlier resPES data[7,8,18]. For MAPI film, with the width of the ionic gap of 4.0 eV, the internal potential Γ corresponds to the voltage regime from -2.0 V up to +2.0 V[6,18]. For Ga_2O_3[8] an $E_{ionicgap}$ of 8.2 eV[7,8] is deduced and the potential Γ is normalized correspondingly[8].

The carrier density $N^{\pi}(\Gamma)$ of the LaPs [$P^{3\pi}$, $P^{1\pi}$] as the mobile charge carriers in the covalent-ionic system can be calculated from Eq. (2)[8]:

$N^{\pi}(\Gamma)[P^{1\pi}] = N^{min}\cdot[\exp\{((1-\Gamma)\cdot E_{ionicgap})/kT\}]^{(1-fi)} = N^{min} \cdot \exp\{(1-f_i)\cdot((1-\Gamma)\cdot E_{ionicgap})/kT\}$ (2), where the term of $N^{min}/N^{max} = 1/\exp\{(1-f_i)\cdot E_{ionicgap}/kT\}$. For the carrier densities of the $P^{3\pi}$ LaPs, the term (1-Γ) has to be substituted by Γ.[8] The covalent fraction $(1-f_i)$ appears as the dimension of the Boltzmann term[8] and it indicates that only multi-atomic quasi-particles can participate. With $f_i = 0.9$ in Ga_2O_3 the dimension of $1/(1-f_i) = 10$ requires that the size of the quasi-particle extends over 10 unit cells, and for the photosensitive perovskite materials with $(0.37 \leq f_i \leq 0.73)$ the size varies between 3.7 and 1.6 unit cells. Once knowing the value of f_i, the carrier density in the BiP-band is related to the material specific value of $N^{valence}$ and spans between N^{max} and N^{min} with $N^{max} = (1-f_i) \cdot N^{valence}$.[8]

C. Similarities in the stability range of BiPs and in field- and photodissociation

The origin of the photosensitivity of the covalent-ionic based systems is discussed on the basis of the carrier densities in the BiP-band as a function of the chemical potential Γ. The quantitative analysis considers that the LaPs – as the carriers to determine the transport properties – are able to pair into charge-neutral BiPs. The n-type $P^{3\pi}$ and the p-

type $P^{1\pi}$ may pair into either $B^{2\pi}$, $B^{4\pi}$, or $B^{6\pi}$ BiPs due to the large polarization clouds and their easy formation of multi-atomic polaronic BiP and LaP species. The field- or photodissociation – controlled by the chemical potential Γ – enables then the changes in $N^{\pi}(\Gamma)$ in the dark and the light I-V characteristics.

In all covalent-ionic systems the chemical potential indicates the stability regime in which the BiPs can be formed by pairing. It must be separated from the space charge limited current (SCLC) range, where the transport is limited by the scattering due to the strong Coulomb interaction between coexisting n-type and p-type LaPs with $[P^{3\pi}] = [P^{1\pi}]$ to maintain the charge neutrality condition. Generally, the specific position of the chemical potential as $\Gamma = \Gamma^*$ defines the sharp transition between this SCLC regime and the stability regime of the $B^{2\pi}$ that enables the photosensitivity.

In the following sections we discuss in more detail the influence of the Γ value on the pairing and dissociation behavior, the contributions of the dipolar contributions V^{light} and V^{pair} to the chemical potential Γ, and the corresponding dissociation mechanisms for the examples of photosensitive perovskites (section D) and UV absorbers (section E). Field-dissociation (in the dark) and photodissociation are effective for all existing BiPs. Independent of their composition they result in $P^{1\pi}$ for $B^{2\pi}$, in $P^{3\pi}$ for $B^{6\pi}$, and in $P^{1\pi}$ (when $V_{bias} < 0$) or in $P^{3\pi}$ (when $V_{bias} > 0$) for $B^{4\pi}$. These pairing/dissociation scenarios are relevant in the systems discussed below.

D. FAPI – a photosensitive visible light absorber

FAPI, as all photosensitive perovskites, has a white-light photosensitivity and the light absorption creates a dipole V^{light} within the IDS (explanation based on optical data

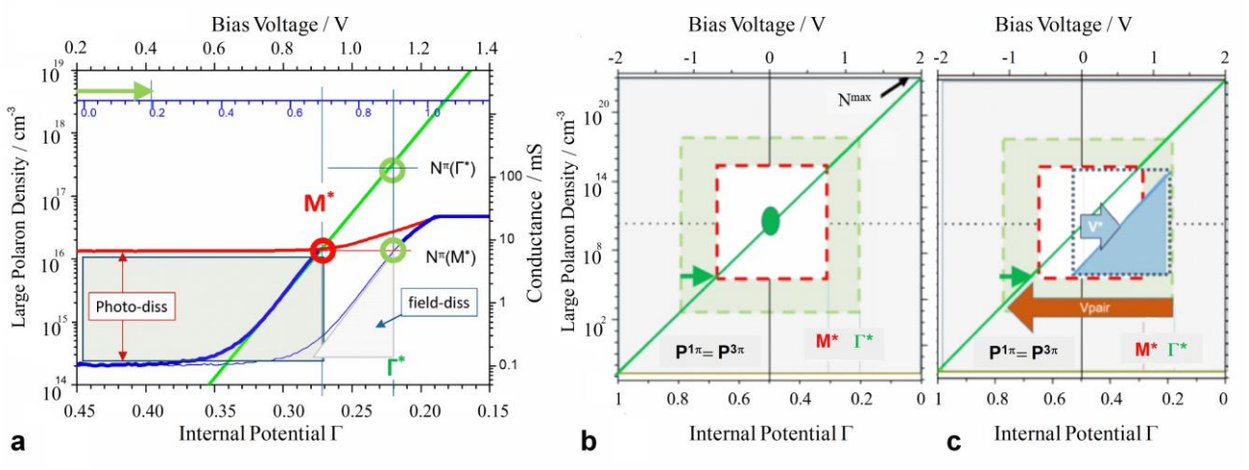

FIG. 2. (a) Analysis of the G-V data (right scale) of FAPI in terms of the $N^{\pi}(\Gamma)$ frame. The figure depicts the as-measured (thin blue), the shifted (bold blue) dark, and the light (red) curves. The critical points of the chemical potential Γ* and M*, and the dipole V* are indicated. (b) The exponential $N^{\pi}(\Gamma)$ dependence (green) is related to the left axis. In this diagram the f_i value of $f_i = 0.62$ corresponds to the exponential slope (green line) that connects N^{max} and N^{min} via N^0 (green bullet). Schematic presentation of the polaronic $B^{2\pi}$ regime created by V^{pair} for Γ* (green dashed) and to M* (red dashed) reduced by V*. (c) Photodissociation occurs within the red dashed box (white area). Field-dissociation occurs within the blue dotted box shifted by V*v for $(V_{bias} + V^*v) > 0$ and it causes the carrier increase along the exponential (blue triangle).

will be discussed elsewhere). In Fig. 2a the corresponding data of FAPI are shown.[6] Our FAPI sample is characterized by the parameters V_{OC} = 1.12V and maximum power of 5.5mW, and shows stable I-V curves from -2.0V to 2.0V.[17] For our analysis, we present the G-V curves by dividing the I-V data with V_{bias}. Further, we use the value of $E^{ionicgap}$ = 4.0 eV and the V_{bias}= 0V corresponding to the mid-gap situation, accordingly. In the G-V curve shown in Fig. 2a the conductance data are given on the right and the corresponding

$N^{\pi}(\Gamma)$ values on the left y-axes. The V_{bias} axis is displayed on the top and the corresponding chemical potential Γ on the bottom x-axis. The value of Γ spans from 1 to 0 for the p-type $P^{1\pi}$ LaPs according to Eq. (1).

The characteristic feature of all photosensitive perovskite devices, i.e., the exponential bias dependence of the dark curve, is observed for V_{bias} close to 1.0V and its slope of 6.8 dec/V is used to determine the f_i value of $f_i = 0.62$[6]. The dark curve (thin blue line) shows the exponential slope that marks the critical point $\Gamma^* = 0.22$ (1.12V) by the intersection with the saturation value of the light curve as shown in Fig. 2a and the slope flatten out when entering the SCLC regime for $\Gamma < \Gamma^*$. The as-measured dark curve (thin blue line) appears with $V_{bias} + V^*v$, and for the quantitative $N^{\pi}(\Gamma)$ analysis it is corrected for V^*v. After this correction, it is shown back-shifted (bold blue line) and refers to the second V_{bias} axis (blue). The second critical point $M^* = 0.27$ (0.92V) is associated with the light curve (red) and appears at $\Gamma = \Gamma^* - V^*$. Fig. 2a reveals that the light, the shifted dark and the $N^{\pi}(\Gamma)$ (thin green line) curves intersect at the M* point. The photoinduced carriers appear when the light dipole V^{light} dissociates the $B^{2\pi}$ BiPs to yield the p-type $P^{1\pi}$ LaPs and their density is given by $N^{\pi}(M^*)$. Therefore, both, the V^{pair} and the V^{light} dipoles determine the photosensitivity. The $N^{\pi}(\Gamma)$ density of the LaPs in dependence on Γ is explained in Fig. 2b with values of $N^{max} = 1.9 \cdot 10^{23} cm^{-3}$ and $N^0 = 1.3 \cdot 10^{10} cm^{-3}$ (dashed horizontal line) at $N^{\pi}(\Gamma = 0.5)$. Generally, the coexisting n-type and p-type LaPs with $[P3\pi] = [P1\pi]$ define the SCLC regime (gray area in Fig. 2b and 2c). Within that regime, the critical points Γ^* and M* demonstrate the interplay of the ionicity factor and the carrier densities under dark and light conditions and are described by $N^{\pi}(M^*)$. Here, the Γ values between Γ^* and $(1-\Gamma^*)$ are visualized by the green dashed box that also defines the

width of the dipole V^{pair} [Γ*, (1-Γ*)] (see Fig. 2c) that creates the photosensitive polaronic regime with $N^{\pi}(\Gamma^*)$ and $N^{\pi}(1-\Gamma^*)$. The green box appears within the SCLC regime as V^{pair} repels the n-type $P^{3\pi}$ LaPs, suppresses the Coulomb interaction, and enables the pairing of $P^{1\pi}$ LaPs into $B^{2\pi}$ BiPs. Thereby, it creates an asymmetric ratio of $P^{1\pi} \gg P^{3\pi}$ ($p \gg n$) and we plot the $N^{\pi}(\Gamma)$ dependence reversed from 1 to 0, hence (refer also to Eq. (2)).

The red dashed box in Fig. 2b and 2c highlights the role of V* that gives the separation between $V = \Gamma^* - M^* = 0.05$ (0.2V) and reduces the size of V^{pair} (the green box) to that of the red boxes in which the BiPs can be stable. Thereby, it limits the photosensitive range of $N^{\pi}(\Gamma)$. Within the red boxes we have to distinguish between photodissociation by V^{light} and field-dissociation by V_{bias}. In the light curve, upon photodissociation all BiPs are dissociated and the $P^{1\pi}$ LaPs contribute to the light curve with the maximum value of $N^{\pi}(M^*)$ of the red dashed box that appears symmetric around $\Gamma = 0.5$ (Fig. 2b).

In the dark curve (blue in Fig. 2a), where only field dissociation is relevant, the dipole V* adds to V_{bias} (illustrated by the blue arrow in Fig. 2c) and it shifts the exponential diagonal in parallel as indicated in Fig. 2c as the blue dotted box. Depending on the respective value of Γ the density of $P^{1\pi}$ LaPs dissociated from $B^{2\pi}$ Bi-polarons increases (blue triangle) up to the maximum value of $N^{\pi}(M^*)$. This value is reached by both, photo- and field-dissociation at their respective Γ values. The rather high N^{π} value of the dark curve (at $\Gamma > 0.4$) is caused by parasitic n-type minority $P^{3\pi}$ carriers that trap p-type majority LaPs and create vagabonding dipole momenta with a zero net moment. They are able to dissociate some of the BiPs and cause the $N^{\pi}(\Gamma)$ value of the dark curve.

They also may possibly contribute to V* as some of them become oriented in the direction of V^{pair} and reduce its value. Fig. 2b visualizes also the relation of the critical parameters Γ*, M*, and V* within the frame of $N^{\pi}(\Gamma)$ with the green dashed box limited by Γ* (see above), with the red dashed box limited by M*, and the blue dotted box shifted by V*, respectively. These three critical parameters appear in all photosensitive perovskite devices and describe the carrier densities $N^{\pi}(\Gamma)$ of the dark and the light curve of individually prepared photosensitive perovskites systems, respectively. The stability regime of the $B^{2\pi}$ is controlled by the value of Γ*, the performance limits by M*, and the loss mechanisms by V*.

In summary, recording the light I-V curve from V_{bias} = 0V towards +1V, the measured current is determined by the photodissociated $P^{1\pi}$ carrier density $N^{\pi}(M^* = \Gamma^* - V^*)$ and it remains at this value for all values of $\Gamma > M^*$ ($V_{bias} < M^*v$ on the voltage axis). In contrast, the dark curve proceeds up to Γ* ($V_{bias} \leq \Gamma^*v$), but the field-dissociation increases also up to the $N^{\pi}(M^*v)$ point, too. Finally, for values of $\Gamma < \Gamma^*$ ($V_{bias} > \Gamma^*v$), the system leaves the polaronic regime. Then, irreversible charge transfer to/from the more localized IDS becomes possible. It leads to the reappearance of the n-type carriers (into the regime with $p \gg n$ defined by V^{pair}) and they cause instabilities/hysteresis of the dark current when the sweep is returned. This difference between the field- and photo-dissociation depends on $V^* = \Gamma^* - M^*$ and it is evident in our model. To the best of our knowledge, it is for the first time reported in the literature and has not been realized and addressed in common analyses, yet. As a matter of fact the difference between the Γ* and the M* values of the chemical potential explains nicely the shift of the dark/light curves in recent Mott-Schottky analyses.[21]

It should be noted that our data analysis goes beyond the common power conversion efficiency analyses of perovskite solar cells using open circuit voltage, short circuit current and fill factor. It unravels the existence of two different transport property regimes, of different internal potentials for the dark and the light curves, predicts the upper and lower limits for photosensitivity, proposes an access to understand the loss mechanisms, and defines the regime for stability and highly reversible charge transport.

E. Ga_2O_3 – a photosensitive UV-absorber

Ga_2O_3 as a solar-blind UV absorber material can be used as a respective photodetector when epitaxially grown on sapphire substrates. The corresponding devices have two interdigitated electrodes with a lateral separation of several µm. The onset of UV-photosensitivity appears, consistent with the electronic structure of Ga_2O_3, at an energy beyond 4.8 eV as the excitation has to overcome the exciton band into the 3 eV broad CT-band[8]. The device performance as well as the optical excitation energies depend on the thickness of the epilayer and best results are obtained for values of about 150 nm with a spectral responsivity of up to 40 A/W at (4.57 eV) 270 nm.[22]

The quantitative analysis of the carrier density $N^{\pi}(\Gamma)$ works in dependence on the chemical potential Γ for this covalent-ionic system as well. The pairing/dissociation scenarios were used to reproduce the experimental results from Ref. 22 and the calculated data are demonstrated in Fig. 3a and 3b. The obtained I-V characteristics of this Ga_2O_3 device are modeled in the same $N^{\pi}(\Gamma)$ scenario as for the FAPI one (described above) by using values for the ionic gap $E^{ionicgap} = 8.2$eV and $f_i = 0.9$, resulting in a slope of about 2 dec/V, both determined from the resPES data.[8] In Fig. 3b, the green dashed box within the $N^{\pi}(\Gamma)$ frame for Ga_2O_3 together with the dark (blue) and the light (golden) carrier

densities $N^{\pi}(\Gamma)$ are shown. The black curve is the blocking curve (with $N_{blocking}$) taken in the rectifier geometry and results from a superposition of the p-type and the n-type rectifier geometries. Fig. 3a shows the same calculated data in commonly used linear plots with the characteristic inverted s-shaped I-V curves.

Ga_2O_3 is a systems with a symmetric doping with the consequence that for $V_{bias} = 0$ the maximum carrier density for both $P^{3\pi}$ and $P^{1\pi}$ LaPs is N^0 (i.e., at $\Gamma = 0.5$ $N^{\pi}[P^{3\pi}] = N^{\pi}[P^{1\pi}]$) and for $V_{bias} \neq 0$ the I-V curve appears symmetric around $V_{bias} = 0$, as shown in linear (Fig. 3a) and particularly in logarithmic (Fig. 3b) presentations. In the almost perfect Ga_2O_3 epilayers, V* is negligible ($V^* \approx 0$) and Γ^* and M* are quasi identical (no existence of the red box). Therefore, it behaves as an ideal system compared to the scenario explained for the FAPI system and pairing is enabled in the green dashed box. Note, that in Fig. 3b the data are plotted for both, the $P^{1\pi}$ and the $P^{3\pi}$ LaPs and the corresponding Γ dependence differs accordingly (Γ for $P^{3\pi}$ and $(1- \Gamma)$ for $P^{1\pi}$, see Eq. (2)). As $V^* \approx 0$, the pairing dipole depends now only on the polarity of V_{bias} and it is active for the pairing of the $P^{1\pi}$ LaPs ($\Gamma < 0.5$) and $P^{3\pi}$ LaPs ($\Gamma > 0.5$), resulting either in $B^{2\pi}$, $B^{6\pi}$, or $B^{4\pi}$ BiPs. When all LaPs are paired, field-dissociation of the BiPs follows the diagonal within the green dashed box with increasing Γ resulting in N^{π} values of up to the N^0. It is limited to the density of N^0 due to the coexistence of n-type and p-type LaPs coming from either n-type $P^{3\pi}$ LaPs for $V_{bias} > 0$ or p-type $P^{1\pi}$ LaPs for $V_{bias} < 0$, respectively. The field-dissociation of the dark curves is illustrated by the green ($P^{3\pi}$) and blue ($P^{1\pi}$) arrows within the green dashed box (Fig. 3b).

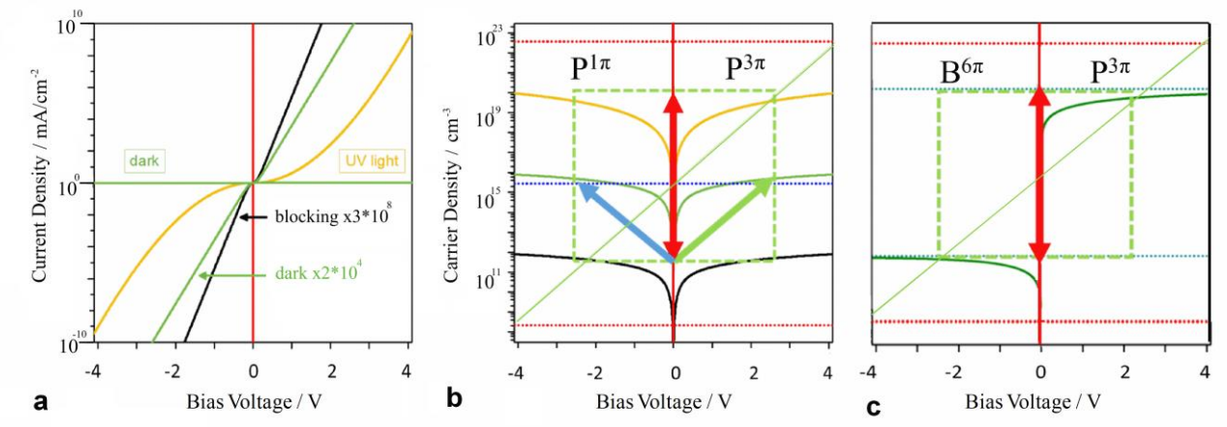

FIG. 3. The calculated blocking (black), dark (blue), and light (golden) curves in linear (a) and logarithmic (b) scales to model the corresponding curves of a solar-blind Ga_2O_3 UV-detector.[8,22] In this presentation the field- and photodissociation mechanisms are visualized together for $P^{1\pi}$ and $P^{3\pi}$ within the green dashed box displayed in (b). The rectifying mode for the $P^{3\pi}$ LaPs is shown in (c).

Photodissociation by V^{light} works for all Γ values within the green dashed box and all BiPs are dissociated as indicated in Fig. 3b (and in Fig. 3c) by the red vertical double sided arrow. The uppermost concentration of the green box is reached for either the $B^{2\pi}/P^{1\pi}$ when $V_{bias} < 0$ or the $B^{6\pi}/P^{3\pi}$ when $V_{bias} > 0$, respectively. Again, V_{bias} determines either p-type or n-type LaPs and the symmetric I-V curves (Figs. 3a and 3b) result from a superposition of the p-type and the n-type rectifier geometries, respectively. The latter is depicted in Fig. 3c giving an asymmetric case for only the n-type $P^{3\pi}$ LaPs. Again, the carrier density of $N^{\pi}(\Gamma^*)$ is reached and an on/off ratio of 10^8 is enabled.

F. Discussion

We emphasize that the analysis based on the chemical potential with its ability to control intrinsic dipoles works for systems with different doping profiles such as p = n or

$p \gg n$. For epitaxial Ga_2O_3 with $p = n$, we established that there is no loss dipole ($V^* = 0$) and no reduction of Γ^* to M^*, hence. The pairing of BiPs still works when $V^{pair} = 0$ as the BiPs are stabilized by the usage of single crystals or epilayers. The stability in Ga_2O_3 is not a problem; the same is true for the reversibility. We therefore suggest that for photosensitive perovskites ($p \gg n$) the dipolar losses appear only when structural defects exist or are enabled. The field- and photodissociation mechanisms of BiPs work for both covalent-ionic systems. Field dissociation occurs in FAPI up to $N^{\pi}(M^*)$ starting at a rather high N^{π} value due to parasitic dipoles, whereas in Ga_2O_3 only up to N^0 due to the coexistence of n-type and p-type LaPs and parasitically dissociated LaPs are negligible. Photodissociation takes place in FAPI up to the limit of the red boxes $N^{\pi}(M^*)$, whereas in Ga_2O_3 even up to $N^{\pi}(\Gamma^*)$ (green box).

Based on our comparative systematic studies on the critical values of the chemical potential we are able to address some of the most striking observations in both, photosensitive perovskites and TCOs. We established the dipolar losses V^* as a novel aspect in the material science, and in our report it appears only in the material class of the perovskites where the value of V^{pair} is crucial for photosensitivity. A possible origin of V^* is the existence of parasitic n-type minority $P^{3\pi}$ carriers that trap p-type majority LaPs and create vagabonding dipole momenta, some of which contribute to V^* when they become oriented and reduce V^{pair}. Actually, our understanding of the loss dipole will open a door for new materials optimization strategies as we found that there is a limited range of reversible charge transfer that may have been ignored in many hitherto reported stability tests and has led to questionable results, hence.

Next, we focus on the characteristic value of the chemical potential $\Gamma = \Gamma^*$ In both covalent-ionic systems it acts as a threshold that limits the range of the carrier densities with the corresponding values of $N^{\pi}(1-\Gamma^*)$ and $N^{\pi}(\Gamma^*)$ that enables photosensitivity and reversible device operation. It defines the window (green dashed boxes) of the polaronic regime where the pairing/dissociation equilibria are free from Coulomb forces. A subsequent lowering in the Γ^* value will cause an improved performance in both covalent-ionic systems. As it appears as the main limiting parameter it should be optimized first before starting the reduction of losses. Hence, it is worthwhile to discuss the possible mechanisms to optimize the individual materials. It is noteworthy, that both FAPI and Ga_2O_3 exhibit a similar value of around $\Gamma^* = 0.2$: the green box for Ga_2O_3 starts at $\Gamma = 0.2$ and for FAPI it starts also at around $\Gamma = 0.2$ (but only if $V^* = 0$). However, right now, it seems that there is no way to reduce this value further in order to remove the limit on available carrier densities. Here, we cannot solve this open issue about the importance of Γ^* and just will give some arguments based on our comparative analyses.

First, in a recent study[23] on a related perovskite system (mesoporous on compact TiO_2 was used) in which three different thicknesses of the triple cation based perovskite where investigate (i.e. 5, 15 and 400 nm), we found a very high value of $\Gamma^* = 0.37$ for initially deposited droplets without a continuous 2-dimensional film network. This value is not a bulk phenomenon as witnessed by simultaneously performed UV-VIS data that exhibited bulk-like features for all film thicknesses. Actually, the value of Γ^* decreased significantly towards $\Gamma^* = 0.2$ as soon as the droplets coagulate upon increasing the coverage and form a continuous film. This gives a strong evidence that the value of Γ^* is

lowered by the lateral strain and reflects the film properties of the perovskite materials. Another evidence for the influence of strain on the value of Γ* is also given for Ga_2O_3. Here, the low value of Γ* = 0.2 is observed only within a narrow range of film thickness that optimizes the strain in the epilayer.[22]

Next, the value of Γ* certainly is not only influenced by the strain in the films. Also the signatures of the ionic subsystem may contribute as they maintain the Coulomb character, for example when the wave functions of the carriers are hybridized with deep valence states (O2s, I4p, Ga3d, Pb5p).

In addition, there may exist compensated ionic defect pairs (Coulomb forces) such as interstitial-vacancy pairs (Ga-interstitial-O-vacancy in Ga_2O_3 or halide-interstitial-halide-vacancy in perovskites). Eventually, these residual ionic contributions cannot be reduced completely as some of them are required to maintain the structural stability of the films and therefore it is not possible to reduce their concentration further and to lower Γ* to values lower than 0.2. Another reason is the size of the wave-functions of the multi-atomic LaPs, it may be restricted by molecular or crystallographic subunits or domains that limit the "true" 2-dimensional film growth.

Therefore, in our approach we present a more physical explanation than questionable attempts that are adopted from Si-based homogeneous covalent semiconductors with Debye lengths of several µm and are forced to be applied for an almost fully ionic system ($f_i = 0.9$) with typical active layer thickness of < 500 nm.

IV. SUMMARY AND CONCLUSIONS

In this contribution, we presented the basic ideas of the dark and light I-V characteristics analysis and compared two systems, i.e. FAPI and Ga_2O_3, as representatives of the covalent-ionic families of perovskites and TCOs, respectively. We find common features based on a similar electronic structure and a large number of IDS. The charge transport carriers are multi-atomic LaPs with their ability for charge neutralization by pairing into BiPs. The main message is that the chemical potential Γ and the related analysis of the carrier densities $N^{\pi}(\Gamma)$ work for both systems, independent on existing large differences in the values of f_i, $E^{ionicgap}$, $\hbar\omega$, and in the spectral sensitivities. The chemical potential Γ is well suited to describe I-V curves in covalent-ionic systems and it is applied for a wide range of f_i values and for a wide range of ionic gaps. The concept is based on spectroscopic analyses of the core levels of resPES data, and subsequently the multi-atomic polaronic scenarios are linked directly to the I-V electrical characteristics. The chemical potential Γ regulates the stability regime and the pairing and dissociation equilibria between BiPs and LaPs of the photosensitive devices based on photosensitive perovskites and TCOs. This description offers a new route to understand the transport properties of covalent-ionic systems in general, and of FAPI and Ga_2O_3 in particular. The scenario with large polarons differs from the descriptions in the single particle picture in which the electron-hole pair formation dominates. Instead, we consider negatively charged LaPs, their net charge is effectively screened by their large polarization cloud and they are able to respond to small changes in the internal chemical potential. Another consequence of such dressed electrons is their tendency to coagulate into aggregates supported by the rather high density ($N^{max} > 10^{22}$ cm^{-3}) and by the

fractional f_i value. This explains the large spatial dimensions of these quasi-particles as the size of the polarization cloud exceeds distinctly that of their unit cell. We deduce that the scenario and analysis presented here with its influence on the carrier densities on the BiP stability regime, and on the loss dipole can be used for the different covalent-ionic systems as the defect bands of their basic electronic structure are similar. Also, the basic mechanisms for photosensitivity are similar, but differences appear for the size of V^{pair}. In FAPI the photosensitivity appears only for $V^{pair} > 0$ and asymmetric doping ($p \gg n$). In Ga_2O_3 with symmetric ($p = n$) doping, pairing is still possible although $V^{pair} = 0$, it works as the polarity of V_{bias} causes pairing or dissociation for either the n-type or the p-type electrode (diode) in the alternating device geometry, respectively.

The analysis of the chemical potential is not only useful to learn about the photosensitive properties of the two covalent-ionic example systems, but it also allows to determine the ranges of reversible operation to avoid instabilities, includes a description of loss mechanisms, and provides a quantitative analysis of carrier densities. Thereby, it offers a novel and powerful tool for optimization strategies for covalent-ionic materials and devices.

ACKNOWLEDGMENTS

Special thanks are delighted to M. Richter and particularly A. Lewerenz for their stimulating discussions during the long-term development of our models for ionicity and charge carrier density determination of mixed covalent-ionic materials. We would further like to acknowledge K. Müller, K. Gawlinska-Necek and E. Pożarowska for fruitful discussions and help during the data analysis and manuscript preparation, as well as the

interest and support of J. I. Flege. This work is partially funded by BMWI, within the ZIM projects KK5087602BR1 and ZF4510602AG7.

AUTHOR DECLARATIONS

Conflicts of Interest

The authors have no conflicts to disclose.

Author Contributions

Małgorzata Kot: Funding acquisition: Supporting; Resources: Lead; Conceptualization: Supporting; Writing – original draft: Supporting, Writing – Review & Editing: Supporting, K. Henkel: Funding acquisition: Lead; Conceptualization: Supporting; Visualization: Supporting; Writing-Original draft: Supporting, Writing – Review & Editing: Supporting, Dieter Schmeißer: Conceptualization: Lead; Formal analysis: Lead; Visualization: Lead; Writing – original draft: Lead.

DATA AVAILABILITY

The data that support the findings of this study are available from the corresponding author upon reasonable request.

REFERENCES

[1]S. Ahmad, S. Kazim, and M. Grätzel, *Perovskite Solar Cells: Materials, Processes, and Devices*, (Wiley-VCH, Weinheim, 2021).

[2]A. M. Oni, A. S.M. Mohsin, Md. M. Rahman, and M. B. H. Bhuian, Energy Rep. **11**, 3345 (2024).

[3]M. Gerosa, F. Gygi, M. Govoni, and G. Galli, Nature Mater. **17**, 1122 (2018).

[4]J. Xu, W. Zheng, and F. Huang, J. Mater. Chem. C **7**, 8753 (2019).

[5]H. Chen et al, Semicond. Sci. Technol. **39**, 063001 (2024).

[6]M. Kot, K. Gawlińska-Nęcek, E. Pożarowska, K. Henkel, and D. Schmeisser, Adv. Sci. (submitted).

[7]D. Schmeißer, and K. Henkel, J. Appl. Phys. **123**, 161596 (2018).

[8]D. Schmeißer, K. Müller, and K. Henkel, J. Phys. Chem. C **127**, 23077 (2023).

[9]M. Kot, M. Vorokhta, Z. Wang, H. J. Snaith, D. Schmeißer, and J. I. Flege, Appl. Surf. Sci. **513**, 145596 (2020).

[10]C. Das, M. Kot, T. Hellmann, C. Wittich, E. Mankel, I. Zimmermann, D. Schmeißer, M. Khaja Nazeeruddin, and W. Jaegermann, Cell Rep. Phys. Sci. **1**, 100112 (2020).

[11]M. Kot, L. Kegelmann, H. Köbler, M. Vorokhta, C. Escudero, P. Kúš, B. Šmíd, M. Tallarida, S. Albrecht, A. Abate, I. Matolínová, D. Schmeißer, and J. I. Flege, ChemSusChem **13**, 5722 (2020).

[12]J. Kruszyńska, J. Ostapko, V. Ozkaya, B. Surucu, O. Szawcow, K. Nikiforow, M. Hołdyński, M. M. Tavakoli, P. Yadav, M. Kot, G. P. Kołodziej, M. Wlazło, S. Satapathi, S. Akin, and D. Prochowicz, Adv. Mater. Interfaces **9**, 2200575 (2022).

[13]D. Schmeißer, K. Henkel, and C. Janowitz, Europhys. Lett. **123**, 27003 (2018).

[14]D. Schmeißer, M. Kot, S. Alberton Corrêa, C. Das, and K. Henkel, "Interface potentials, intrinsic defects, and passivation mechanisms in Al_2O_3, HfO_2, and TiO_2 ultrathin films," in *Encyclopedia of Interfacial Chemistry: Surface Science and Electrochemistry*, edited by K. Wandelt (Elsevier, Oxford, 2018), Vol. 3.1.

[15]L. Pauling, *The Nature of the Chemical Bond* (Cornell University Press, New York, 1960).

[16]J.C. Phillips, Rev. Mod. Phys. **42**, 317 (1970).

[17]S. Sahayaraj, Z. Starowicz, M. Ziółek, R. Socha, Ł. Major, A. Góral, K. Gawlinska-Necek, M. Palewicz, A. Sikora, T. Piasecki, T. Gotszalk, and M. Lipinski, Materials **16**, 5352 (2023).

[18]M. Kot, K. Wojciechowski, H. J. Snaith, and D. Schmeißer, Chem.–Eur. J. **24**, 3539 (2018).

[19]Y. Zhou, Y. Yin, Y. Peng, W. Zhou, H. Yuan, Z. Qin, B. Liu, Y. Zhang, and D. Tang, Mater. Res. Express **1**, 025025 (2014).

[20]M. Hossein, S. Pal, S. Masanta, K. Dasgupta, T. Maity, K. Sarkar, P. Kumar, S. Bysakh, and P. Pal, Optical Materials **135**, 113322 (2023).

[21]I. Zonno, A. Martinez-Otero, J.-Ch. Hebig, and T. Kirchartz, Phys. Rev. Applied **7**, 034018 (2017).

[22]D.J. Rogers, P. Bove, X. Arrateig, V. E. Sandana, F. H. Teherani, M. Razeghi, R. McClintock, E. Frisch, and S. Harel, in Oxide-Based Materials and Devices IX, Proceedings of SPIE edited by D.J. Rogers, C. D Look, F.H. Teherani, SPIE, 2018; p 105331.

[23]C. Das, R. Roy, M. Kedia, M. Kot, W. Zuo, R. Félix, T. Sobol, J. I. Flege, and M. Saliba, ACS Appl. Mater. Interfaces **15**, 56500 (2023).